# UWB Path Loss Models for Ingestible Devices

Sofia Perez-Simbor, Carlos Andreu, Concepcion Garcia-Pardo, Matteo Frasson, Narcis Cardona, *Member, IEEE*[1]

***Abstract*— Currently, some medical devices such as the Wireless Capsule Endoscopy (WCE) are used for data transmission from inside to outside the body. Nevertheless, for certain applications such as WCE, the data rates offered by current medical frequency bands can result insufficient. Ultra Wideband (UWB) frequency band has become an interesting solution for this. However, to date, there is not a formal channel path loss model for the UWB frequency band in the gastrointestinal (GI) scenario due to the huge differences between the proposed studies. There are three main methodologies to characterize the propagation channel, software simulations and experimental measurements either in phantom or in *in vivo* animals. Previous works do not compare all the methodologies or present some disagreements with the literature. In this paper, a dedicated study of the path loss using the three methodologies aforementioned (simulations, phantoms and *in vivo* measurements) and a comparison with previous researches in the literature is performed. Moreover, numerical values for a path loss model which agrees with the three methodologies and the literature are proposed. This paper aims at being the starting point for a formal path loss model in the UWB frequency band for WBANs in the GI scenario.**

***Index Terms*— UWB, WBAN, in-body, Wireless Capsule Endoscopy, Propagation Channel, Path Loss, Gastrointestinal, *in vivo*, phantoms.**

## I. Introduction

Wireless Capsule Endoscopy (WCE) has become a good alternative for conventional endoscopy, allowing the detection of diseases in some regions like the small bowel or colon, with the recording and transmission of images. Nevertheless, the current low data rate transmission in the WCE only allows the transmission of low quality images [1]. Higher data rates would allow the streaming transmission of high quality images or videos, which are a necessity to ease the recognition of diseases and enable the localization and tracking of the capsule [2].

Currently, the standard IEEE 802.15.6-2012 [3] is used for the regulation of wireless medical devices in Wireless Body Area Networks (WBANs). The standard considers the narrowband Medical Implant Communications Service (MICS) band, from 402 – 405 MHz as the optimum for implanted (in-body) to surface (on-body) communications (IB2OB). This frequency band has good propagation behavior and achieves a small size for the antennas. Moreover, another narrowband band defined in the IEEE 802.15.6-2012 standard from 2.4 to 2.4835 GHz (included in the ISM band from 2.4 – 2.5 GHz) is proposed for on-body to on-body (OB2OB) and on-body to external (OB2OFF) communications[1,2].

Ultra Wideband (UWB) frequency band, covering from 3.1 to 10.6 GHz, is also defined in the IEEE 802.15.6-2012 standard for the communications from OB2OB or OB2OFF. This band is characterized for a very low power consumption, smaller size of the antennas and higher data rate [4].

Even though those are the defined frequencies for the different scenarios, many works have studied the optimum frequency bands for IB2OB communications[5]–[7]. Some results consider the optimum bands to be below or around 1 GHz. However, these results do not take into account some of the current necessities for the medical technology. As mentioned before, the low power transmission or the data rate that for some applications e.g., the WCE, needs to be higher Therefore, as described in the IEEE standard, the maximum data rates for MICS and ISM frequency bands are 455 kbps and 971 kbps respectively, whereas for UWB frequency band 12.636 Mbps are defined [3]. Moreover, the smaller size of the antennas, as well as the power consumption, are some desirable characteristics for the future ingestible devices.

For these reasons, recent investigations [8]–[10], are considering the UWB frequency band as a possible candidate to substitute the MICS band for high data rate communications for implanted devices in WBANs. UWB frequency band is also characterized by the high attenuation suffered by the transmitted signal when it propagates across the human tissues. Furthermore, such attenuation is frequency-dependent due to the variation with frequency of the electromagnetic properties of the human body tissues [11], [12]. Thus, a proper channel characterization is a key factor to consider the UWB frequency band as the future of WBANs.

The three main methods to characterize the propagation channel in the WBANs are through numerical software-based simulations [13], [14], and experimental measurements either in laboratory environment with phantoms [15], [16] or through *in vivo* experiments [17]–[20]. Each method has different strengths and weaknesses: Software-based simulations are easy to perform, and they are available for everybody through commercial software e.g., CST® MWS®, ANSYS® HFSS. Nevertheless, the high complexity of the simulations, the high computational time and the unreal conditions of the simulations drive to the conclusion that this methodology itself is not enough to properly characterize a WBAN channel.

This paper was submitted for review on February 28th of 2018, revised on November 1st of 2018 and accepted on 12th December of 2018. This work was supported by the European Union's H2020:MSCA:ITN program for the "Wireless In-body Environment Communication- WiBEC" project under the grant agreement no. 675353. This work was also funded by the Programa de Ayudas de Investigación y Desarrollo (PAID-01-16) from Universitat Politècnica de València and by the Ministerio de Economía y Competitividad, Spain (TEC2014-60258-C2-1-R), by the European FEDER funds

S. Perez-Simbor, C. Andreu, C. Garcia-Pardo and N. Cardona are with the Universitat Politècnica de València in the Instituto de Telecomunicaciones y Aplicaciones Multimedia (iTEAM), Valencia, Spain.

M. Frasson is with the Hospital Universitari i Politècnic La Fe, Digestive Diseases Area, Valencia, Spain.

[1] The mentioned standard defines more narrow frequency bands than the MICS and ISM. Nevertheless, those are the most widely used among the scientific community and manufacturers

*In vivo* experiments are performed in hospitals or laboratories with facilities adapted for these experimental purposes. These measurements are the most similar to a real case because they take into account all the tissues, blood and internal movements among other factors that appear in the living bodies. On the contrary, since the animal is alive, a proper location of the antenna and the control of the environment is a challenging work. Moreover, there are many ethical restrictions regarding the experimentation with living animals [21]. Lastly, the so-called phantom measurements are becoming a good alternative to *in vivo* experimentation, reducing the animal experimentation. In general, phantoms are created to emulate certain characteristics of the human body [22], [23], e.g., color, texture, size, weight. For the case of propagation in WBANs, the electromagnetic (EM) properties of the human tissues [15], [24], [25] – reported in [26] – are the desired parameters to mimic. Unfortunately, phantoms in the UWB frequency band are not easy to achieve and plenty of researches are performed using phantoms that were not accurate enough [15], [18]. However, in [27]–[29], authors used novel accurate phantoms that properly mimic the human tissues in the spectrum from 0.5 to 26.5 GHz [25], [30], and are protected by patent [31]. In addition, the measurement setup should be designed for the IB2OB scenario in order to avoid some inaccuracies such as the bad isolation of the measurement environment. Thus, in [32] phantom measurements were performed with accurate phantoms and a testbed specifically designed for the purpose of IB2OB scenario in the WBANs.

In addition, in the GI scenario, some existing works are only focused in one methodology or sometimes two of them, such as in [18], [29], where a comparison between *in vivo* experiments and phantoms are performed. Therefore, to the best of the authors' knowledge, there are no studies in the literature reporting a comparative study between the results obtained from the three methodologies in the GI scenario. Moreover, the current literature regarding channel characterization is not homogeneous, i.e., different frequency bands, distance range and antennas are considered for each study. Thence, there is a lack of a unified PL model for the GI part of the human body.

In this paper, a comparative study between the three methodologies aforementioned (software simulations, *in vivo* and experimental measurements with phantoms) is presented. Moreover, the three setups considered for the three methodologies are intended to mimic the real applications of the IB2OB GI scenario. Like the WCE, where the transmitting antenna is located inside the intestine of the human body and the receiving antenna is placed over the abdominal region of the human body. Moreover, simulations and experiments are designed to be as similar between them as possible. The research performed in [32], with heterogeneous accurate phantom is extended here and results are compared with realistic *in vivo* experiments. As a result, path loss (PL) models considering the three methodologies are given and compared. Finally, a comparative study of different PL models already presented in the literature is discussed.

The reminder of this paper is as follows: in section II the methodology used for each measurements type is described, section III presents the results obtained for all the methodologies and the path loss model values. Section IV presents the discussion with previous literature. Lastly, the conclusion of this paper is given in section V.

## II. Measurement and Methodology

### A. Scenario of interest

In IB2OB scenario, the antennas used for the communications are highly affected by the human tissues surrounding them. Thus, antennas should be designed for this particular scenario, either implanted transmitting antenna [23], [33] or on-body receiving antenna [34], [35]. In Fig. 1, the antennas used for this work are shown. Concretely, the on-body antenna is a quasi-omnidirectional antenna in the UWB frequency band for on-body communications with 5 cm and 4.4 cm length and width respectively [36]. The in-body antenna has a smaller size, 2.3 cm × 2 cm, also with a quasi-omnidirectional radiation pattern in the UWB frequency band. Such antenna has been designed and miniaturized taking into account the surrounding body tissues as detailed in [28].

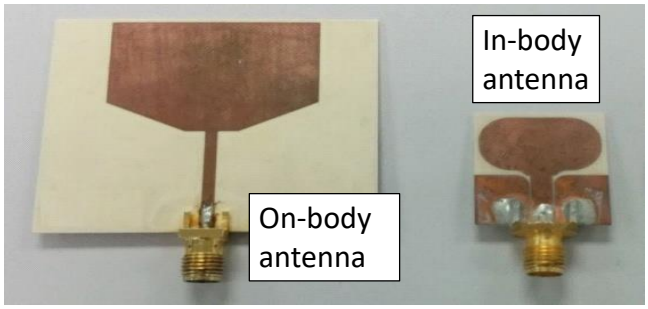


Fig. 1. On-body and in-body antenna [28].

### B. Phantom measurements

In the gastrointestinal scenario, the main tissues involved in the signal transmission are: large or small bowel, muscle, fat, skin and blood. In Fig. 2(a) and (b) the dielectric constant and conductivity given by [26] for such tissues are plotted.

As one can observe, muscle, colon and small bowel have similar dielectric constant and conductivity in the low UWB frequency band. Considering this issue and for the sake of simplicity these three tissues will be considered as only one. Hereinafter, muscle phantom tissue will be employed for simulations and phantoms measurements. However, for *in vivo* experiments since the proper placement of the in-body antenna is an arduous task, the location either in colon or small bowel is considered indistinctly

In Fig. 3, the setup used for the phantom measurements is shown. The setup consists of a small anechoic chamber designed for frequencies above 1.3 GHz (Fig. 3, element. 1). Inside the anechoic chamber, a magnetic tracker (Fig. 3, element 4a), a 3D Cartesian positioner (Fig. 3, element 2a), a multilayer phantom container (Fig. 3, element 5), and the transmitting and receiving antennas (Fig. 1) are placed.

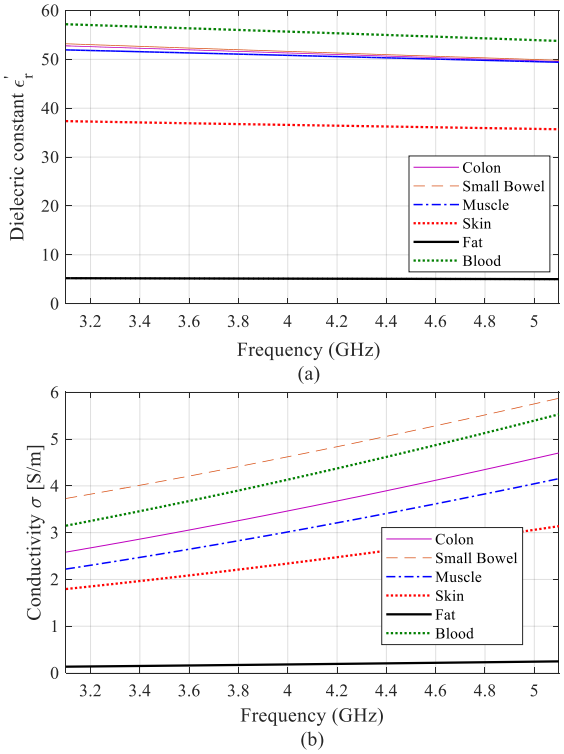


Fig. 2. (a) Dielectric constant and (b) Conductivity of the human tissues given by Gabriel at [26]

The multilayer phantom container consists of a squared container with two layers of 23 cm × 25 cm × 25 cm and 2 cm × 25 cm × 25 cm, filled with muscle phantom [30] and fat phantom [25], [37] respectively. The dielectric constant and the conductivity of both phantoms are depicted in [32] they show a high level of agreement compared with the literature. Concretely, a deviation of less than 1% for both parameters is achieved for the muscle phantom, whereas 4% and 12% of deviation are reached for the dielectric constant and conductivity of the fat phantom.

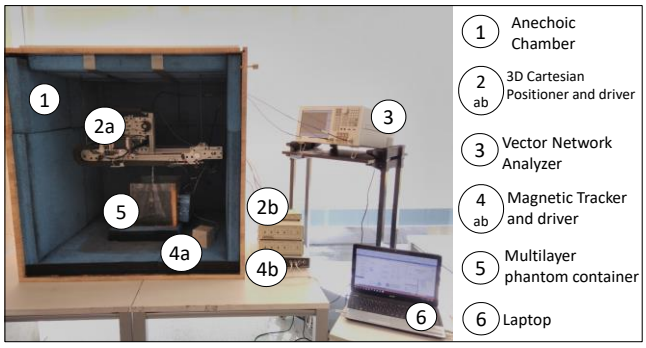


Fig. 3. Full setup used for phantom measurements in [32].

The 3D Cartesian positioner precisely places the transmitting antenna inside the phantom container (264 positions), concretely inside the muscle layer. The receiver is located over the external wall of the fat layer. The receiver position is shifted over the fat layer wall to mimic the multi-receiver case. Finally, the 3D magnetic tracker (*Ascension Technology Corporation, trakStar* with a *Mid-Range Transmitter*) creates a magnetic field thanks to a magnetic transmitter located inside the anechoic chamber. Two magnetic sensors are attached to both antennas, giving the exact distance between antennas.

Table I column 1 summarizes the configuration parameters of the VNA for the phantom measurements. A detailed explanation of this measurement setup, as well as further details, can be found in [32].

TABLE I.
VNA PARAMETERS

| | *Phantom measurements* | *In vivo measurements* |
|---|---|---|
| Resolution points | *N = 3201* | *N =1601* |
| Frequency band | *f = [3.1, 8.5] GHz* | *f = [3.1, 6] GHz* |
| IF Bandwidth | $f_{if}$ *= 3 kHz* | $f_{if}$ *= 3 kHz* |
| Output Power | *P = 8 dBm* | *P = 8 dBm* |

### C. *In vivo measurements*

The *in vivo* experiment was performed in a living porcine model in the facilities of the Hospital Universitari i Politècnic la Fe, Valencia, Spain. Pigs and humans have similar GI conditions, either in size and distribution of the organs, thus these animals are commonly used for digestive experimentation. This experiment was conducted for digestive surgeons and the method used to perform the surgery in the animal was a laparoscopy. Moreover, the *in vivo* measurements were designed to be as similar as possible to the phantom measurements aforementioned.

Fig. 4 shows the laparoscopy performed in the abdominal cavity of the pig. As seen, four incisions were performed: Fig. 4 element 1 to insert the in-body antenna and the cable; Fig. 4, element 2 to insert the gas ($CO_2$) used to inflate the abdominal cavity of the pig and Fig. 4, elements 3a and 3b to insert the laparoscope itself and the laparoscopic instruments, e.g., graspers, to precisely move the antenna to the place under interest.

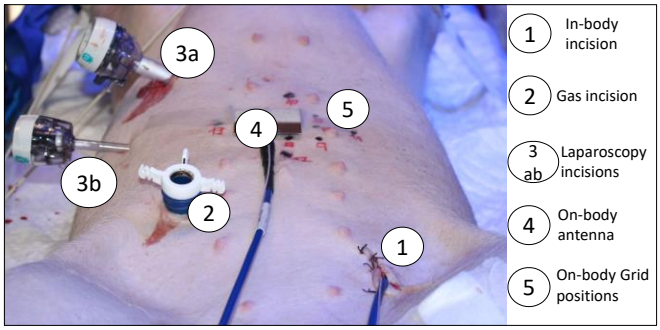


Fig. 4. *In vivo* Measurement setup. Detailed view.

Again, measurements were based on a Vector Network Analyzer (VNA), where the in-body and on-body antennas (Fig. 1) are connected to the port 1 and 2 of the VNA through coaxial cables. In addition, the same 3D magnetic tracker as in phantom measurements with two sensors attached to both antennas was used in the surgical procedure. In Table I second column the configuration parameters of the VNA for the *in vivo* measurements are given.

From measurements, the forward transmission coefficient ($S_{21}$) for different IB2OB positions was calculated. Besides, 5

(a) (b) (c)

Fig. 6. In-body positions (a) In-body position 1 (Tx1), (b) In-body position 2 (Tx2), (c) In-body positions 3 (Tx3).

snapshots of the $S_{21}$ are taken per each IB2OB position and then the average value of such coefficient is calculated. The magnetic tracker also computes 100 positions per each IB2OB position, which are also averaged. In addition, the dynamic range for this configuration was found to be 100 dB.

In Fig. 4, a general view of the receiver grid over the pig is shown. The grid of the positions of the on-body antenna used over the abdomen of the pig is detailed in Fig. 5.

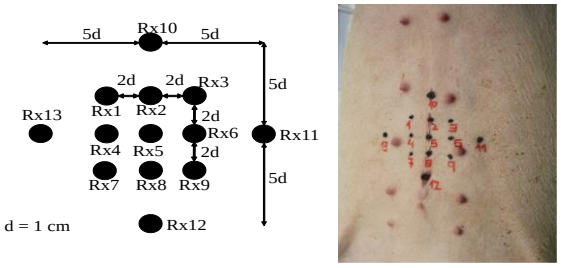


Fig. 5. On-body grid for *in vivo* experiment.

Such on-body grid consists of 13 receiving positions (Rxs). They are placed considering the real case where different receivers are located in different positions over the abdomen. It should be mentioned, that the $CO_2$ used for the laparoscopy is removed once the transmitting antenna is placed in the desired position. Therefore, the measurements are done without any gas, closer to the real case.

Regarding the in-body antenna, 3 different in-body positions, were considered. Since the scenario of interest is mainly the GI tract of the animal, the in-body positions were located to be surrounded by either colon or small bowel indistinctly. Fig. 6 shows the pictures of the in-body positions taken during the surgical procedure. Tx1 and Tx3 (Fig. 6(a) and (c) respectively) are surrounded by small bowel, whereas Tx2 (Fig. 6(b)) is surrounded by small bowel and colon.

### *D. Simulations*

Software simulations were performed with the commercial software CST® MWS®, hereinafter CST. For these simulations, the Time Domain (TD, transient) solver was chosen. Concretely, this software uses the Finite Integration Technique (FIT) as a numerical method to calculate the electromagnetic fields of a certain setup and, in our case, the S-parameters. Simulations were undertaken to confirm the values deduced from phantom and *in vivo* measurements. With this aim, two different configurations were considered:

A) The experimental testbed of Fig. 3 is replicated in CST. More information about this simulation design can be found in [32].

B) The abdominal part of a human female CAD model (Nelly) was chosen to confirm whether the measurements in a living pig were well performed. It should be mentioned that to reduce the complexity of the simulation, only the skin, fat and muscle of the human body was considered, as shown in Fig. 7. Besides, in order to have the most accurate result, cells with a mesh size ranging from an edge length of 0.14 to 2.61 mm were used for these simulations.

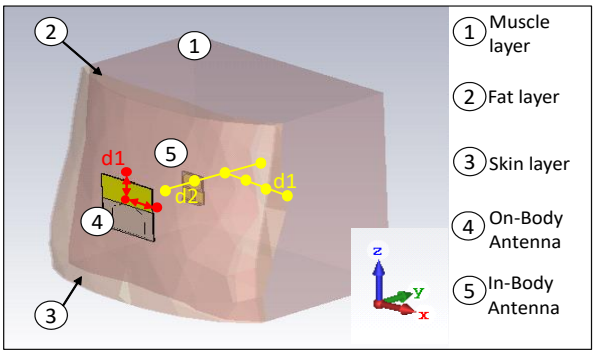


Fig. 7. CST Human CAD model, Nelly and the in-body and on-body grid used.

In case B simulations, the in-body and on-body antennas were located in different positions along X, Y, and Z axes. Fig. 7 depicts these different positions. The on-body antenna is placed in 3 different positions over the skin layer of the CAD model Nelly. For the in-body antenna, 6 in-body positions were considered as shown in Fig. 7. Thus, a total range of distances between in-body and on-body antennas ranging from d = 4 cm to 7.95 cm is achieved.

## III. Results

### *A. Antenna Matching*

As mentioned before, the antenna matching varies with the surrounding tissues. Therefore, the reflection coefficient ($S_{11}$) of either in-body and on-body can vary depending on its location, especially in real configuration. In Fig. 8, the absolute value of the $S_{11}$ is shown for *in vivo* measurements considering the three transmitting positions (Tx1, Tx2, Tx3) and three on-body receiving positions.

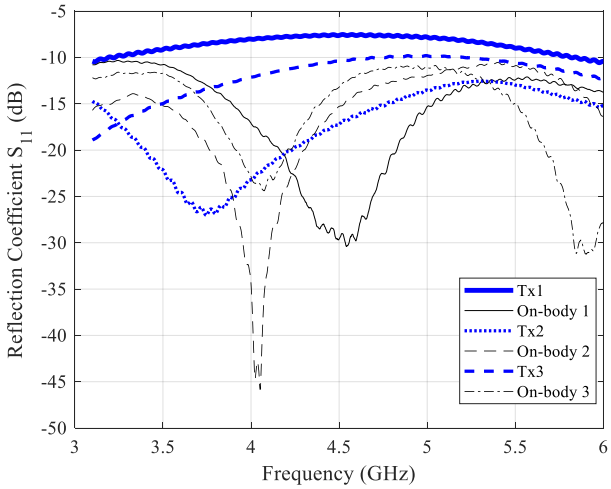


Fig. 8. Reflection coefficient parameters for different in-body and on-body positions at *in vivo* measurements.

As can be observed, the reflection coefficient of the in-body and on-body antenna varies depending on the position of the antenna, i.e., Tx1 and Tx3 show similar response (both are surrounded with small bowel), while Tx2 has slightly different shape. In any case, the $S_{11}$ has a maximum value of -7 dB for Tx1, for which, we consider this antenna matched as well as in [20], where the antenna is considered matched for a value below -6 dB for *in vivo* experiments.

The on-body matching is also shown, with the reflection coefficient plotted for 3 different on-body positions. As seen, the on-body reflection coefficient is always below -10 dB. Moreover, in [32], the reflection coefficient for the in-body and on-body antenna are plotted, showing a high level of agreement either in the shape and values of the curve with those represented in Fig. 8.

### *B. Channel transfer function*

The N-points channel transfer function in frequency domain can be deduced from measurements as $H(f)=|S_{21}|e^{-j\theta_{S_{21}}}$ being $|S_{21}|$ and $\theta_{S_{21}}$ the module and the phase of the forward transmission coefficient ($S_{21}$) given by the VNA and $f$ the frequency. In Fig. 9, the channel transfer function is depicted for different in-body and on-body positions from 3.1 to 6 GHz.

One can observe how as the distance between antennas becomes larger, the response of the channel transfer function above the noise floor (-90 dB in terms of relative received power) decreases, and thus, the useful bandwidth. So, from Fig. 9, distances above d = 7.62 cm and frequencies above $f$ = 5.1 GHz, the signal is considered to be under the noise floor level. Therefore, for further analysis, a trade-off between the maximum distance between antennas and the maximum useful bandwidth should be achieved. Hereinafter, the frequency band considered is 3.1-5.1 GHz and the larger distance is d = 8 cm. These results agree with the literature in which the low UWB frequency band is studied [17], [38].

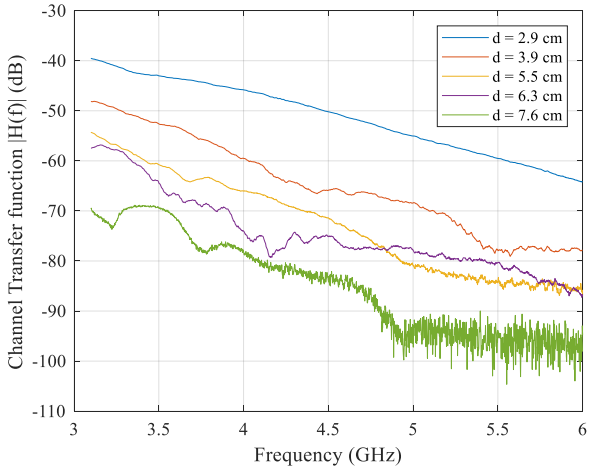


Fig. 9. Channel transfer function for *in vivo* values.

In addition, the simulations with the CST CAD model Nelly (case B) were also performed and compared with the channel transfer function in *in vivo* measurements (Fig. 10). It should be mentioned that simulations were performed only for the desired frequency band, i.e., 3.1 to 5.1 GHz in order to reduce the computational cost.

Fig. 10 also shows that the slope of the channel transfer function is very similar for similar distances between antennas. It is important to take into account that inside the pig, the exact tissues between antennas are unknown.

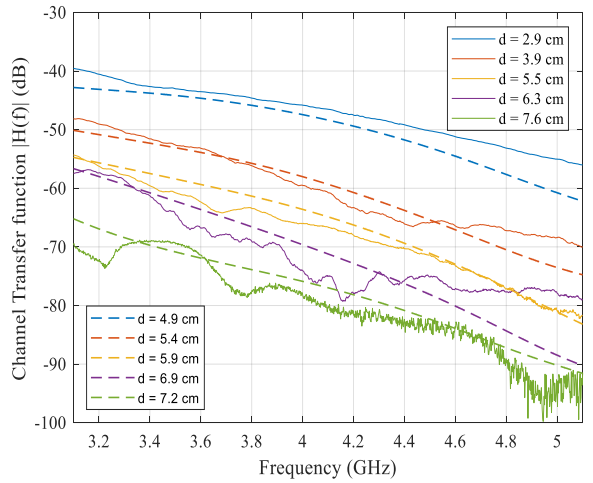


Fig. 10. Comparison of H(f) for *in vivo* (solid) measurements and software simulations (Case B) (dashed).

In this comparison, it is possible to see the high similarities between the results performed with both methodologies as well as in [32], where the phantoms measurements were compared with software simulations (Case A). In that case, when the antennas were completely aligned and perfectly matched with the simulations, the results were very similar. Same occurs here, where the comparison between *in vivo* and simulations (Case B) shows a high level of matching, validating the *in vivo* measurements

### *C. Path Loss*

The path loss (PL) is obtained from the channel transfer function as:

$$PL(dB) = -10\log_{10}\left(\sum_{i=1}^{N}\frac{\left(\left|H(f_i)^2\right|\right)}{N}\right) \quad (1)$$

Fig. 11 illustrates the path loss as a function of the distance for the *in vivo* and numerical simulations with Nelly (Case B). In this work, the antenna behavior is considered, being thus, a radio link budget evaluation. However, in literature the term path loss is commonly used.

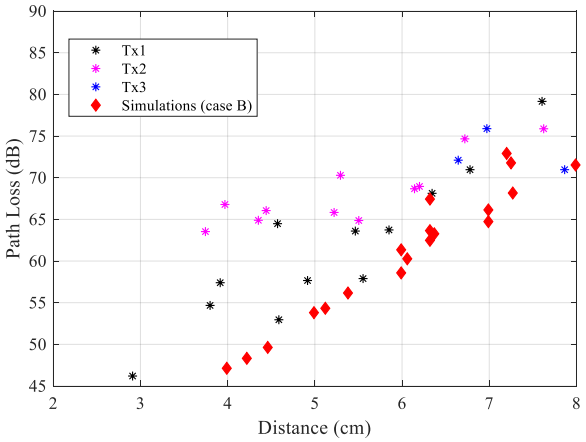


Fig. 11. Path loss model values for the *in vivo* and numerical simulations (Case B)

One can observe how the PL values given by the numerical simulations are few decibels below those deduced from the *in vivo* measurements. This slightly mismatch is given for all the contributions that appear in real experiments, i.e., reflections inside the pig, blow flow, respiration etc., which are not considered in the numerical simulations. Moreover, in simulations, both antennas are faced, whereas in *in vivo* measurements a perfect alignment between antennas is difficult to achieve. Same occurs in [32], where the values of the numerical simulations (case A) are lower than experimental measurements in phantom.

In order to obtain a general path loss model, phantom measurements have to be taken into account for the large number of positions obtained and the real external conditions of the measurements. For this purpose, Fig. 12 represents the path loss values obtained from multilayer phantom measurements in [32], together with the *in vivo* measurements and software simulations (Case B)

From Fig. 12 a similar trend and path loss values between the three configurations can be observed. Nevertheless, the data values obtained from the multilayer phantom container have a shift of two centimeters in the X axis. It should be highlighted that the experiments performed in phantom measurements considered muscle and a 2 cm width of fat phantom layer. As depicted in Fig. 2, the conductivity of the fat is very low, barely affecting the attenuation of the signal. As a consequence, the distance used for this model can be changed regarding the quantity of abdominal fat. To confirm this, a new phantom measurement campaign was performed using only homogeneous muscle phantom and using the same frequency band (3.1 to 5.1 GHz) and the same antennas.

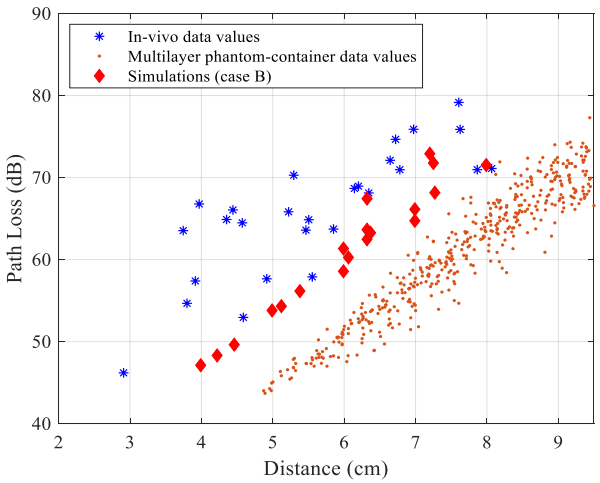


Fig. 12. Path Loss for *in vivo*, software simulations and multilayer phantom-container.

Fig. 13(a) shows the comparison between the multilayer and the homogenous phantom-container measurements. As seen, in Fig. 13(b), where the multilayer measurements are 2 cm shifted for the distance from 3 to 6 cm approximately, the PL values between both measurements are very similar. The multilayer has about an average PL data value of 2 to 3 dBs above the homogenous PL, which is due to the extra losses introduced by the fat.

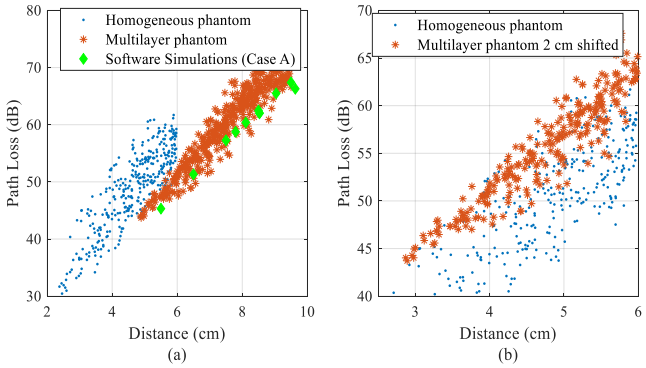


Fig. 13. Homogeneous vs heterogeneous path loss models. (a) Original PL data values and CST phantom design simulations (case A) (b) Multilayer PL data values 2 cm shifted

Therefore, from the results obtained with this comparative, the measurements performed with fat phantom, can be shifted up to 2 cm to the left (Fig. 13(b)) in order to replicate as much as possible the *in vivo* results, where the pig has less than 2 cm of abdominal fat. In addition, in Fig. 13(a)) the results from simulations (case A) are shown. These data values correspond to the software design mimicking the experimental phantom measurements. As seen, phantom measurements and software simulations show a high level of agreement, being the simulation values in the lower part of data cloud in phantom. As discussed in [32] this is for the perfect alignment and perfect conditions considered in simulations, which are not always easy to achieve in real measurements.

Finally, in Fig. 14, the comparison between the *in vivo* measurements, shifted phantom measurements and software simulations (Nelly model, case B) are shown. In this case, the

agreement between results coming from the three methodologies is clearly shown. Therefore, a more general PL model can be deduced from the results.

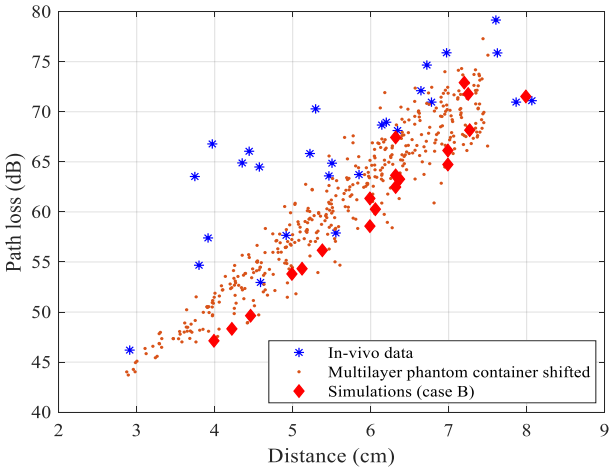


Fig. 14. Path Loss data values for CST, *in vivo* and phantom measurements shifted

### D. Path Loss Models

The most accurate fitting model should be determined in order to achieve the best fitting to the samples. Although the most common path loss model is the logarithmic one [39], some other works in literature have proposed a linear fitting [17]. Equations (2) and (3) describe the logarithmic and linear PL models. The logarithmic PL model is given by:

$$PL(dB) = 10\gamma \log_{10}\left(\frac{d}{d_0}\right) + PL_0(dB) + \mathrm{X}(\sigma,\mu) \qquad (2)$$

being $d$ the separation between antennas, $d_0$ the reference distance, $PL_0(dB)$ the reference PL value at the reference distance ($d_0$), $\gamma$ the logarithmic path loss exponent and $\mathrm{X}(\sigma,\mu)$ the statistical distribution modeling the shadowing term of the signal. Such statistical distribution typically follows a Gaussian model with mean, $\mu$, and standard deviation of $\sigma$. In the same manner, the linear model is given by:

$$PL(dB) = \alpha\left(\frac{d}{d_0}\right) + PL_0(dB) + \mathrm{X}(\sigma,\mu) \qquad (3)$$

where, $\alpha$ is the slope of the line. It should be mentioned that the maximum distance achieved for simulations, phantom measurements and *in vivo* measurements is not exactly the same. In the case of the *in vivo* experiments the maximum distance measured is $d_{max}$ = 8.067 cm. For the multilayer phantom model is $d_{max}$ = 9.5 cm or $d_{max}$ = 7.5 cm (if the samples are shifted 2 cm due to the fat layer). In software-based simulations, the maximum distance d = 7.95 cm. Results are shown in Table II where the Root Mean Squared Estimator (RMSE) is computed for both the linear and logarithmic method, for the three methodologies. Measured path loss models and fitting models are plotted in Fig. 15.

From the Table II, the results with logarithmic and linear model seem to be unalike. Nevertheless, for all the models the RMSE have similar values. In Fig. 15 it is possible to visually realize the similarities between models for the range of given distances.

TABLE II.
PATH LOSS MODELS

| | Logarithmic | Linear |
|---|---|---|
| *In vivo* | $PL_0$=26.2266 dB<br>$d_0$ = 1 cm<br>$\gamma$ = 5.3967<br>$\mu \approx 0$<br>$\sigma$ = 4.4972<br>RMSE = 28.1 | $PL_0$= 41.5635 dB<br>$d_0$ = 1 cm<br>$\alpha$ = 4.337<br>$\mu \approx 0$<br>$\sigma$ = 4.6007<br>RMSE = 28.8 |
| CST Nelly model (Case B) | $PL_0$ =-8.3767 dB<br>$d_0$ = 1 cm<br>$\gamma$ = 8.9681<br>$\mu \approx 0$<br>$\sigma$ =1.9795<br>RMSE = 7.5 | $PL_0$= 19.7445 dB<br>$d_0$ = 1 cm<br>$\alpha$ = 6.8262<br>$\mu \approx 0$<br>$\sigma$ = 1.9489<br>RMSE = 7.37 |
| Phantom | $PL_0$ =-29.7593 dB<br>$d_0$ = 1 cm<br>$\gamma$ = 10.3395<br>$\mu \approx 0$<br>$\sigma$ = 2.3069<br>RMSE = 3.64 | $PL_0$ = 13.8201 dB<br>$d_0$ = 1 cm<br>$\alpha$ = 6.1719<br>$\mu \approx 0$<br>$\sigma$ = 2.2724<br>RMSE = 3.54 |
| Phantom shifted | $PL_0$ = 6.29 dB<br>$d_0$ = 1 cm<br>$\gamma$ = 7.3824<br>$\mu \approx 0$<br>$\sigma$ = 2.3772<br>RMSE = 3.88 | $PL_0$ = 26.1639 dB<br>$d_0$ = 1 cm<br>$\alpha$ = 6.1719<br>$\mu \approx 0$<br>$\sigma$ = 2.2724<br>RMSE = 3.51 |

Regarding the comparison between methodologies. The shifted phantom model and the simulations (Case B) are very similar, as shown for the $\alpha$ and $\gamma$ values. The *in vivo* measurements show slightly different results, as expected from the data values. Nevertheless, all the three trends are very similar.

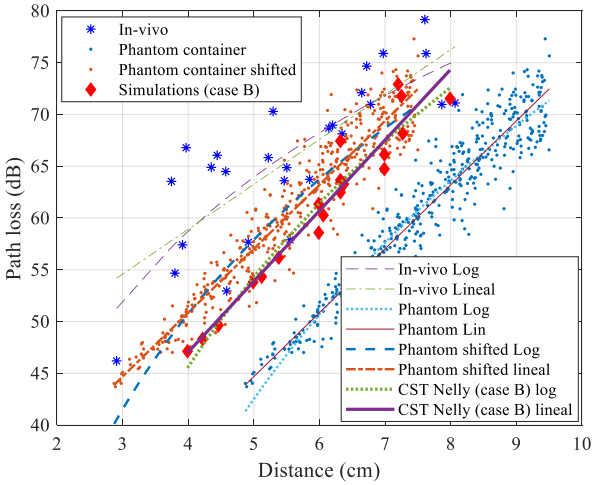


Fig. 15. Path Loss measured and simulated data along with their fitted linear and logarithmic models

Therefore, from the given distance range (3 to 8 cm) and the given frequency band (3.1 to 5.1 GHz), we can assume that the exponential factor either in the logarithmic or linear model varies from $\gamma$ = 5.4 to 8.9 and $\alpha$ = 4.3 to 6.8 and the standard deviation of the scattering $\sigma$ = 2 to 4.6 dB, for both models.

## IV. Discussion

In this section, the similarities with other PL models already presented in literature are discussed. As already mentioned, the PL is highly affected by the location of the antenna in the human body due to the different EM properties of the human tissues, as well as by the antenna characteristics, which cannot be de-embedded from measurements. Therefore, only PL models for the abdominal region or muscle tissue will be taken into account, regardless of the antennas used.

In [11] a first approach of comparison was studied. However, a comparison between some path loss models regardless of the model and the methodology used is performed. From this work, we have chosen the PL models with similar characteristics as the described here, i.e., same distance, frequency, scenario and mathematical model (logarithmic or linear) to evaluate the discrepancies or similarities between the already presented and our models. For our case of study, the logarithmic models for simulations, *in vivo* and phantoms are chosen to standardize with the literature, since mostly all the models are logarithmic.

Fig. 16 shows the PL models within a distance range from 3 to 8 cm and a frequency range between 3.1 to 5.1 GHz and considering abdominal or gastrointestinal scenario. It should be mentioned that some models have an initial distance value above 3 cm. In these cases, the PL model is only represented for their defined distance range.

In Fig. 16(a), the PL models as a result of software simulations are studied. Concretely, in [38], (Y. Shimizu et al.), some simulations are performed in the abdominal region for a frequency band from 3.4 to 4.8 GHz and defined from a distance range from 5 to 9 cm. This model and ours (dotted line) have a high level of agreement, with similar increasing trend. In [40] (Shi et al.) simulations are also performed from the same frequency band as Shimizu but for a distance range from 2 to 24 cm. For this study, 3 curves are depicted because the authors proposed 3 different PL models regarding the position of the receivers. One can observe an evident difference between models. Our model and the models defined by Shi have a quite different slope. This is due to the large distance range (22 cm) defined at [40]. In Fig. 16(b), the experimental PL models obtained either for phantom measurements or *in vivo* measurements are depicted. In [27] (Andreu et al), homogeneous phantoms measurements are performed. The frequency band starts at 3.1 to 8.5 GHz and the distance range vary from 5.5 to 20 cm. In [17] (Garcia-Pardo et al) homogeneous phantom and *in vivo* measurements are compared. In this case, the selected frequencies vary from 3.1 to 5 GHz, the distance range from 5 to 11 cm. In addition, it is the only linear model presented. Finally, two other experimental models presented by Shimizu et al in [19] are depicted. Again, the frequency band selected is from 3.4 to 4.8 GHz and the distance range from 3 to 12 cm. Two models are presented because they performed measurements with one antenna but two different polarization. In Fig. 16(b), it is possible to see how the *in vivo* model presented by Garcia-Pardo and our proposed phantom model, have a high level of agreement although the in-body antennas used were not the same. Moreover, our proposed *in vivo* model shows a quasi-perfect matching with the presented model by Shimizu 2 (also deduced from *in vivo* measurements and with different antennas). Moreover, the logarithmic exponent given by Shimizu 2 (*in vivo*) and Garcia-Pardo (*in vivo*) $\gamma_{Shimizu}$ = 5.2 (logarithmic) and $\alpha_{Garcia\text{-}Pardo}$ = 5.2 (linear), match with our given values in the previous section.

In addition, it should be remarked that the models proposed by Andreu [27] and Shi in [40] are given for larger distance ranges than the other models: 14.5 and 22 cm respectively. And both of them present a large disagreement with other models presented in literature.

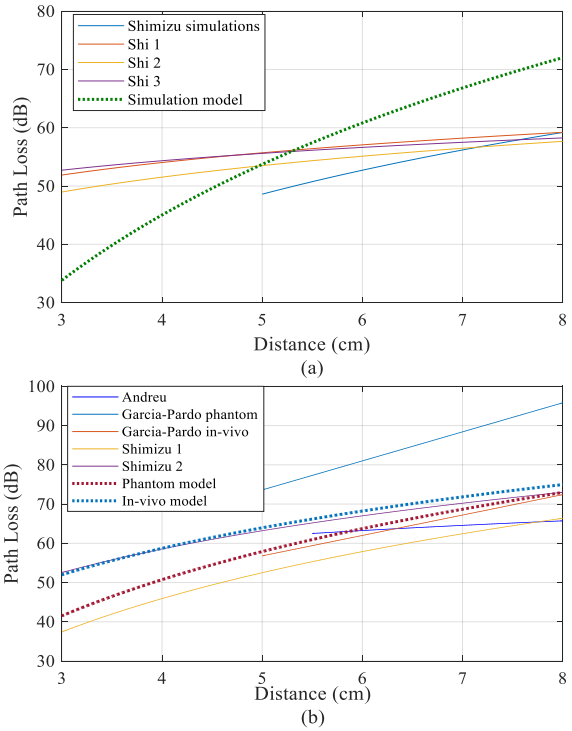


Fig. 16. Comparison between proposed and presented models found in literature (a) Simulations (b) Experimental measurements

## V. Conclusions

In this paper, the radio channel in a gastrointestinal scenario in the lower part of the UWB frequency band (3.1-5.1 GHz) is studied. Some novelties are presented in this paper. Firstly, the path loss models are computed using three different methodologies for the channel characterization, i.e., software simulations, experimental measurements in multilayer phantom and *in vivo* realistic experiments. Then, for each methodology linear and logarithmic path loss models were evaluated. As a result, it was shown that the measured path loss data values obtained from the three methodologies have a high level of agreement between them in terms of losses as a function of distance. In addition, it was found that the width of fat present in the body affects the model since the distance between antennas increases while not the losses.

Comparing our results with others already proposed in the literature in the gastrointestinal scenario, and in the same frequency band (3.1-5.1 GHz) some interesting conclusions were obtained: in simulations, phantoms and *in vivo* measurements the closest models were those with similar conditions while the antennas used seem not to have a decisive

impact in the results. However, those with the same antennas but larger distance range or different frequency band showed higher disagreement

For all of this, we can conclude that for the gastrointestinal scenario, for a distance range from 3 to 8 cm and a frequency band of 3.1 to 5.1 GHz the path loss exponent is in between 4.3 to 6.8 and 5.4 to 8.9 for linear and logarithmic models respectively. It should be highlighted that such results were supported by *in vivo* measurements in a very realistic case where three different positions of the small bowel and colon were considered.

In-body communications in UWB frequency band are still an open topic for future research. First, the improvement of phantom measurement setups to make them more similar to a real *in vivo* scenario is an open issue. In addition, more *in vivo* values are needed to obtain more data values, which lead to more accurate PL models. Furthermore, more measurements using different kinds of antennas are necessary to confirm these findings and generalize them. Because, as deduced from the results in section IV not only the antennas but other variables such as the tissues or the frequency range impact on the channel characteristics. For the best of our knowledge, there are no works focused on the channel characterization using different in-body antennas and considering different methodologies of analysis (software, phantom measurements and *in vivo* measurements). Finally, a deeper study about how the frequency could influence the received signal in the UWB frequency band is needed.

## REFERENCES


[1] G. Ciuti, A. Menciassi, and P. Dario, "Capsule Endoscopy : From Current Achievments to Open Challenges," *IEEE Trans. Biomed. Eng.*, vol. 4, pp. 59–72, 2011.

[2] M. Barbi, S. Perez-Simbor, C. Garcia-Pardo, C. Andreu, and N. Cardona, "Localization for capsule endoscopy at UWB frequencies using an experimental multilayer phantom," in *2018 IEEE Wireless Communications and Networking Conference Workshops, WCNCW 2018*, 2018, pp. 390–395.

[3] IEEE Standards Association, "IEEE Standard for Local and metropolitan area networks - Part 15.6: Wireless Body Area Networks," 2012.

[4] A. F. Molisch, "Ultra-Wide-Band Propagation Channels," *Proc. IEEE*, vol. 97, no. 2, pp. 353–371, 2009.

[5] L. C. Chirwa, P. A. Hammond, S. Roy, and D. R. S. Cumming, "Electromagnetic radiation from ingested sources in the human intestine between 150 MHz and 1.2 GHz," *IEEE Trans. Biomed. Eng.*, vol. 50, no. 4, pp. 484–492, 2003.

[6] D. Nikolayev, M. Zhadobov, P. Karban, and R. Sauleau, "Electromagnetic Radiation Efficiency of Body-Implanted Devices," *Phys. Rev. Appl.*, vol. 9, no. 2, p. 24033, 2018.

[7] A. S. Y. Poon, S. O'driscoll, and T. H. Meng, "Optimal frequency for wireless power transmission into dispersive tissue," *IEEE Trans. Antennas Propag.*, vol. 58, no. 5, pp. 1739–1750, 2010.

[8] R. Chávez-Santiago, A. Khaleghi, I. Balasingham, and T. A. Ramstad, "Architecture of an ultra wideband wireless body area network for medical applications," in *Applied Sciences in Biomedical and Communication Technologies, ISABEL*, 2009, vol. 1, pp. 1–6.

[9] Q. Wang, K. Masami, and J. Wang, "Channel modeling and BER performance for wearable and implant UWB body area links on chest," *Proc. - 2009 IEEE Int. Conf. Ultra-Wideband, ICUWB 2009*, pp. 316–320, 2009.

[10] A. Khaleghi, R. Chávez-Santiago, and I. Balasingham, "Ultra-wideband statistical propagation channel model for implant sensors in the human chest," *IET Microwaves, Antennas Propag.*, vol. 5, no. 15, p. 1805, 2011.

[11] C. Garcia-Pardo *et al.*, "Ultrawideband Technology for Medical In-Body Sensor Networks: An Overview of the Human Body as a Propagation Medium, Phantoms, and Approaches for Propagation Analysis," *IEEE Antennas Propag. Mag.*, vol. 60, no. 3, pp. 19–33, 2018.

[12] A. F. Demir, Z. E. Ankaralı, Q. H. Abbasi, E. Serpedin, and H. Arslan, "In Vivo Communications: Steps Toward the Next Generation of Implantable Devices," *IEEE Veh. Technol. Mag.*, vol. 11, no. June, pp. 32–42, 2016.

[13] J. Wang and Q. Wang, "Channel modeling and BER performance of an implant UWB body area link," in *2009 2nd International Symposium on Applied Sciences in Biomedical and Communication Technologies*, 2009, pp. 1–4.

[14] A. Khaleghi, R. Chavez-Santiago, and I. Balasingham, "An improved ultra wideband channel model including the frequency-dependent attenuation for in-body communications," in *Proceedings of the Annual International Conference of the IEEE Engineering in Medicine and Biology Society, EMBC*, 2012, pp. 1631–1634.

[15] H. Yamamoto, J. Zhou, and T. Kobayashi, "Ultra wideband electromagnetic phantoms for antennas and propagation studies," *IEICE Trans. Fundam. Electron. Commun. Comput. Sci.*, vol. E91–A, no. 11, pp. 3173–3182, 2008.

[16] Divya Kurup, W. Joseph, G. Vermeeren, and L. Martens, "In-body Path Loss Model for Homogeneous Human Tissues," *IEEE Trans. Electromagn. Compat.*, vol. 54, no. 3, pp. 556–564, 2012.

[17] C. Garcia-Pardo *et al.*, "Experimental ultra wideband path loss models for implant communications," *2016 IEEE 27th Annu. Int. Symp. Pers. Indoor, Mob. Radio Commun.*, pp. 1–6, 2016.

[18] D. Anzai *et al.*, "Experimental evaluation of implant UWB-IR transmission with living animal for body area networks," *IEEE Trans. Microw. Theory Tech.*, vol. 62, no. 1, pp. 183–192, 2014.

[19] Y. Shimizu, D. Anzai, R. Chavez-Santiago, P. A. Floor, I. Balasingham, and J. Wang, "Performance Evaluation of an Ultra-Wideband Transmit Diversity in a Living Animal Experiment," *IEEE Trans. Microw. Theory Tech.*, pp. 1–11, 2017.

[20] P. A. Floor *et al.*, "In-body to on-body Ultrawideband propagation model derived from measurements in living animals," *IEEE J. Biomed. Heal. Informatics*, vol. 19, no. 3, pp. 938–948, 2015.

[21] E. Parliament and C. of the E. Union, "Directive 2010/63/EU of the European Parliament and of the Council of 22 September 2010 on the protection of animals used for scientific purposes," *Off. J. Eur. Union*, pp. 33–79, 2010.

[22] L. Januszkiewicz and S. Hausman, "Simplified human phantoms for narrowband and ultra-wideband body area network modelling," *Compel-the Int. J. Comput. Math. Electr. Electron. Eng.*, vol. 34, no. 2, SI, pp. 439–447, 2015.

[23] T. Karacolak, A. Z. Hood, and E. Topsakal, "Design of a dual-band implantable antenna and development of skin mimicking gels for continuous glucose monitoring," *IEEE Trans. Microw. Theory Tech.*, vol. 56, no. 4, pp. 1001–1008, 2008.

[24] S. Castello-Palacios, C. Garcia-Pardo, A. Fornes-Leal, N. Cardona, and A. Valles-Lluch, "Tailor-Made Tissue Phantoms Based on Acetonitrile Solutions for Microwave Applications up to 18 GHz," *IEEE Trans. Microw. Theory Tech.*, 2016.

[25] S. Castelló-palacios, C. Garcia-pardo, A. Fornes-leal, N. Cardona, and A. Vallés-lluch, "Full-Spectrum Phantoms for cm-Wave and Medical Wireless Communications," in *European Conference on Antennas and Propagation, EUCAP*, 2017, pp. 1–3.

[26] C. Gabriel, "Compilation of the Dielectric Properties of Body Tissues at RF and Microwave Frequencies.," *Environ. Heal.*, vol. Report No., no. June, p. 21, 1996.

[27] C. Andreu, S. Castello-Palacios, C. Garcia-Pardo, A. Fornes-Leal, A. Valles-Lluch, and N. Cardona, "Spatial In-Body Channel Characterization Using an Accurate UWB Phantom," *IEEE Trans. Microw. Theory Tech.*, 2016.

[28] C. Andreu, C. Garcia-Pardo, A. Fornes-Leal, M. Cabedo-Fabrés, and N. Cardona, "UWB In-Body Channel Performance by Using a Direct Antenna Designing Procedure," in *11th European Conference on Antennas and Propagation (EUCAP)*, 2017, p. 5.

[29] C. Garcia-Pardo, R. Chavez-Santiago, N. Cardona, and I. Balasingham, "Experimental UWB frequency analysis for implant communications," in *Proceedings of the Annual International Conference of the IEEE Engineering in Medicine and Biology Society, EMBS*, 2015, vol. 2015–Novem, pp. 5457–5460.

[30] S. Castelló-Palacios, C. Garcia-Pardo, A. Fornes-Leal, N. Cardona, and A. Vallés-Lluch, "Tailor-Made Tissue Phantoms Based on Acetonitrile Solutions for Microwave Applications up to 18 GHz," *IEEE Trans.*

*Microw. Theory Tech.*, vol. 64, no. 11, pp. 3987–3994, 2016.
[31] N. Cardona, S. Castelló Palacios, A. Fornés Leal, C. García Pardo, and A. Vallés Lluch, "Synthetic Model of Biological Tissues for Evaluating the Wireless Transmission of Electromagnetic Waves," Patent WO/2017/109252, 2017.
[32] S. Perez-Simbor, M. Barbi, C. Garcia-Pardo, S. Castelló-Palacios, and N. Cardona, "Initial UWB In-Body Channel Characterization Using a Novel Multilayer Phantom Measurement Setup," in *IEEE Wireless Communications and Networking Conference, WCNC*, 2018, p. 6.
[33] Q. Wang, D. Plettemeier, and X. Fang, "Impedance Characteristics and Field Separation of Body Implanted Antennas," in *International Conference on Body Area Networks, BodyNets '16*, 2016, p. 7.
[34] X. Fang, M. Ramzan, Q. Wang, and D. Plettemeier, "Compact Antipodal Vivaldi Antennas for Body Area Communication," in *nternational Conference on Body Area Networks, BodyNets '17*, 2017, p. 7.
[35] A. Pellegrini *et al.*, "Antennas and propagation for body-centric wireless communications at millimeter-wave frequencies: A review," *IEEE Antennas Propag. Mag.*, vol. 55, no. 4, pp. 262–287, 2013.
[36] C. Tarin, P. Marti, L. Traver, N. Cardona, J. A. Diaz, and E. Antonino, "UWB channel measurements for hand-portable devices: A comparative study," *IEEE Int. Symp. Pers. Indoor Mob. Radio Commun. PIMRC*, 2007.
[37] M. Lazebnik, E. L. Madsen, G. R. Frank, and S. C. Hagness, "Tissue-mimicking phantom materials for narrowband and ultrawideband microwave applications.," *Phys. Med. Biol.*, vol. 50, no. 18, pp. 4245–58, Sep. 2005.
[38] Y. Shimizu, D. Anzai, T. Furukawa, and J. Wang, "Performance improvement by transmit diversity technique for implant ultra-wideband communication," *IET Microwaves, Antennas Propag.*, vol. 10, no. 10, pp. 1106–1112, 2016.
[39] K. Sayrafian-Pour, W.-B. Yang, J. Hagedorn, J. Terrill, K. Yekeh Yazdandoost, and K. Hamaguchi, "Channel Models for Medical Implant Communication," *Int. J. Wirel. Inf. Networks*, vol. 17, no. 3–4, pp. 105–112, 2010.
[40] J. Shi and J. Wang, "Channel characterization and diversity feasibility for in-body to on-body communication using low-band UWB signals," *2010 3rd Int. Symp. Appl. Sci. Biomed. Commun. Technol. ISABEL 2010*, pp. 1–4, 2010.

**Sofia Perez-Simbor** received her M.Sc. degree in telecommunications engineering from the Universitat Politècnica de València in 2016. She is currently pursuing the PhD degree in the Research Institute of Telecommunications and Multimedia Applications (iTEAM) of the Universitat Politècnica de València.

From 2015 to 2016 she was a Special Research Student at the Mie University, Tsu, Japan, where she carried out her Master Thesis. Her research is focused in the experimental channel characterization for in-body communications in UWB frequencies.

**Carlos Andreu** was born in Valencia, Spain. He received the M.Sc. degree in telecommunication engineering and the PhD degree from the Universitat Politècnica de València in 2013 and 2018, respectively.

His research is focused on the in-body channel characterization within high frequencies, as well as on the study of diversity-based techniques to improve the in-body propagation channel performance. His interests also include the design of tiny implantable antennas for enhancing the current wireless healthcare systems

**Concepción García-Pardo** attended the Universidad Politécnica de Cartagena, where she received the M.Sc. degree in Information Technologies and Communications in 2008. In 2012, she received her PhD degree from the Universidad Politécnica de Cartagena, and PhD degree in Microwaves and Microtechnologies from the Lille 1 University.

In 2012, she joined the Research Institute of Telecommunications and Multimedia Applications (iTEAM) of the Universitat Politècnica de Valencia, Spain, where she works as senior researcher. She is author of more 40 publications of journal and conference papers related to wireless communications. She is also part of the management committee of COST Action CA 15104-IRACON. Her current work is focused on wireless medical devices and wireless communications for body area networks.

**Dr. Matteo Frasson** obtained the Specialization in General and Digestive Surgery in 2009. He obtained the Fellowship in Colorectal Surgery in 2010 and the PhD in Medicine in 2013 from the University of Valencia, Spain.

He is currently an Assistant Professor of the University of Valencia, Chief of the Research Group in Digestive Surgery of the Research Institute La Fe and Consultant Colorectal Surgeon in the University Hospital La Fe, Valencia, Spain. He has published 70 full articles in international peer-reviewed journals. His research activity is currently focused on colorectal cancer, anastomotic leak, gene therapy for inflammatory bowel diseases and the use of electromagnetic waves for cancer early detection.

Dr. Frasson is Chairperson of the Young group of the European Society of Coloproctology and Secretary of the Colorectal Section of the Spanish Association of Surgeon and member of the executive committee of the Spanish Society of Coloproctology.

**Narcis Cardona** is with the Communications Department of the Universitat Politècnica de València, Spain. Since 1990, where he became Full Professor in 2006. He is the Head of the Mobile Communications Group and the Director of the Research Institute of Telecommunications and Multimedia Applications (iTEAM) of the Universitat Politècnica de València. His current research interests include mobile channel characterization, broadcast cellular hybrid networks, and body area networks.

Prof. Cardona is author of 10 patents, several research books and more than 200 publications in international journals and conferences of the communications field. He has been Chair of the WG3 in COST2100, General Chair of COST IC1004 and Vice-Chairman of COST IC15104 IRACON since 2016. He is also member of the Steering Committee of METIS (7FP), and METIS-II (H2020).